

Chapter One

Introduction

1.1 BLACK HOLES IN NATURE

Because of their brilliance, black holes give us a unique view of our universe at both the smallest and largest scales. Masses of candidate black holes associated with astrophysical sources include¹ $\sim (3\text{--}10)M_{\odot}$ black holes found in our Galaxy, intermediate-mass ($\sim(10^2\text{--}10^4)M_{\odot}$) black holes observed in nearby galaxies, massive ($\sim(10^5\text{--}10^7)M_{\odot}$) black holes found in the centers of relatively nearby (redshift $z \lesssim 1$) galaxies, and supermassive ($\sim(10^8\text{--}10^9)M_{\odot}$) black holes at all redshifts (from $z \ll 1$ to $z > 7$). Moreover, newly formed black holes are thought to power the intense emissions from gamma-ray bursts² (GRBs) that occur in galaxies at all distance scales, from relatively nearby galaxies within 10^2 Mpc to structures at redshifts $z > 8$.

A supermassive black hole found at the center of an active galaxy can shine more brightly than all the stars in the galaxy. Whereas the total starlight power from a large spiral galaxy like the Milky Way may reach $\approx 10^{45}$ ergs s^{-1} , the total luminous powers of the nuclei of active galaxies, called active galactic nuclei (AGNs), commonly exceed $\sim 10^{44}$ ergs s^{-1} . The very brightest AGNs can have *apparent* isotropic bolometric powers exceeding 10^{49} ergs s^{-1} ; apparent because the radiation may be directed into a small fraction of the full sky, so that the actual luminosity is reduced by a beaming factor related to the solid angle into which the emission is radiated. Apparent isotropic GRB powers can exceed $\sim 10^{52}$ ergs s^{-1} . Jet sources from candidate black holes are often most luminous at γ -ray energies, and a variety of phenomena supports a picture of relativistic bulk plasma outflow powered by a black-hole engine.

A fundamental question is the power source of the luminous, energetic emissions from black holes. The energy sources are essentially limited to accretion and black-hole rotation. For matter accretion, dissipation of

¹One Solar mass $M_{\odot} \cong 2 \times 10^{33}$ g. The Solar luminosity $L_{\odot} \cong 4 \times 10^{33}$ ergs s^{-1} . See Appendix E.

²A glossary and acronym list is given in Appendix F.

Table 1.1 Electron and Proton Rest Mass Energies, and Units of Energy

$m_e c^2 = 8.187 \times 10^{-7} \text{ ergs} = 1.236 \times 10^{20} \text{ Hz} = 5.93 \times 10^9 \text{ K}$
$m_e c^2 = 5.11 \times 10^5 \text{ eV} = 511 \text{ keV} = 0.511 \text{ MeV} \cong 0.5 \times 10^{-3} \text{ GeV}$
$\cong 0.5 \times 10^{-6} \text{ TeV}$
$1 \text{ eV} = 2.418 \times 10^{14} \text{ Hz} = 1.602 \times 10^{-12} \text{ ergs}$
$1 \text{ MeV} \cong 1.6 \times 10^{-6} \text{ ergs} = 2.418 \times 10^{20} \text{ Hz} \simeq 10^{10} \text{ K}$
$1 \text{ TeV} \cong 2.4 \times 10^{26} \text{ Hz} \cong 1.6 \text{ ergs}$
$m_p c^2 = 1.5032 \times 10^{-3} \text{ ergs} = 2.27 \times 10^{23} \text{ Hz} \simeq 10^{13} \text{ K}$

gravitational potential energy releases 5–30% of the rest-mass energy, depending on the spin of the black hole and how the angular momentum is deposited at the disk inner edge. The diversity of black-hole spectral states suggests that a parameter at least as important as the total black-hole mass accretion rate, \dot{M} , also plays a role. This could be the spin parameter of the black hole. Rather than describe emissions formed by quasi-spherical accretion or disk accretion onto black holes, which are likely to be quasi-thermal and are well reviewed in a number of books [1–3], here we concern ourselves with the high-energy radiation from black holes associated with relativistic jetted outflows. We consider whether the electromagnetic process can effectively extract energy from a rotating black hole to make luminous black-hole jet emissions, and other high-energy cosmic-ray and neutrino radiations. For this purpose, a formulation of general relativity is developed to understand black-hole electrodynamics and the Penrose process operating near black holes.

The theory of γ -ray emission in black-hole sources cannot be separated from the theory of synchrotron radiation, because the same electrons that Compton-scatter soft photons to γ -ray energies also radiate synchrotron photons at radio and optical frequencies. The lepton acceleration process would likewise accelerate baryons. Ultra-high-energy cosmic ray nucleons are subject to photohadronic losses, accompanied in some cases by the formation of baryonic resonances that decay into photons, leptons, neutrons, and neutrinos. To understand the underlying connections between the accelerated particles that radiate γ rays and neutrinos and those particles that become cosmic rays requires knowledge of the underlying astrophysical processes.

The goal of this monograph is to provide a systematic presentation of the theory of black-hole physics and nonthermal, high-energy radiation mechanisms. We investigate the hypothesis that the most luminous and highest-energy radiations in nature are powered by rotating black holes.

The high-energy universe of nonthermal particles and radiations begins where the hot universe leaves off: when the concept of temperature breaks down. Thermal processes involve particle distributions that are described by the Maxwell-Boltzmann form. The relativistic Maxwell-Boltzmann distribution is given by

$$\frac{dn_{\text{MB}}(p)}{dp} \equiv n_{\text{MB}}(p) = n_0 \frac{p^2 \exp(-\gamma/\Theta)}{\Theta K_2(1/\Theta)} \quad (1.1)$$

[4], where the dimensionless temperature $\Theta = k_{\text{B}}T/m_e c^2$, m_e is the rest mass of the electron (table 1.1), n_0 is the particle number density (particle number and energy densities are generally denoted by lower-case symbols), and $K_2(x)$ is a modified Bessel function of the second kind of order 2 (see Appendix B). Throughout we write the total energy E of a particle of mass m in terms of the particle Lorentz factor $\gamma = E/mc^2$, so that the particle's kinetic energy is $(\gamma - 1)mc^2$, and the particle's (dimensionless) momentum $p = \beta_{\text{par}}\gamma$, where $\beta_{\text{par}} = \sqrt{1 - \gamma^{-2}}$.³ Because relativistic particles are mainly considered, we will frequently take the $\gamma \gg 1$, $\beta_{\text{par}} \rightarrow 1$ asymptote. The particle Lorentz factor will be denoted by γ in the fluid frame, except when we consider problems involving multiple species of particles, where the Lorentz factors of the different species must be distinguished.

At relativistic temperatures, $\Theta \gg 1$, the electron-positron pair production rate increases in proportion to the square of the particle density while the pair annihilation rate declines. Pairs begin to multiply without limit above some fixed temperature ≈ 20 MeV [5,6], requiring ever-increasing energy input. Steady thermal plasmas therefore cannot exist at tens of MeV temperature and higher. Moreover, gases with temperatures $\gtrsim 10$ MeV cannot relax to a Maxwell-Boltzmann distribution, because the bremsstrahlung energy-loss rate dominates the Coulomb thermalization collision rates [7]. (Though both are proportional to the particle number densities, bremsstrahlung energy losses increase with particle energy and elastic Coulomb processes decrease with particle energy.) Thus there is no demonstrated way for the gas to thermalize. Plasma processes are often invoked to achieve rapid thermalization on a timescale related to the inverse of the plasma frequency, but special properties of the waves are required to give a quasi-thermal particle distribution. If a system of characteristic size R containing electrons with density n_e has Thomson depth $\tau_{\text{T}} = n_e \sigma_{\text{T}} R \gtrsim 1$, which is required to obtain large luminosities from small regions, then no steady, thermal plasmas with temperatures $\gg 1$ MeV can exist. Allowed system luminosities and total Thomson depths, including pairs, bifurcate into a normal and pair-dominated branch below a maximum critical temperature for fixed

³The term $\beta = \sqrt{1 - \Gamma^{-2}}$ is preserved for the β factor of bulk plasma outflow.

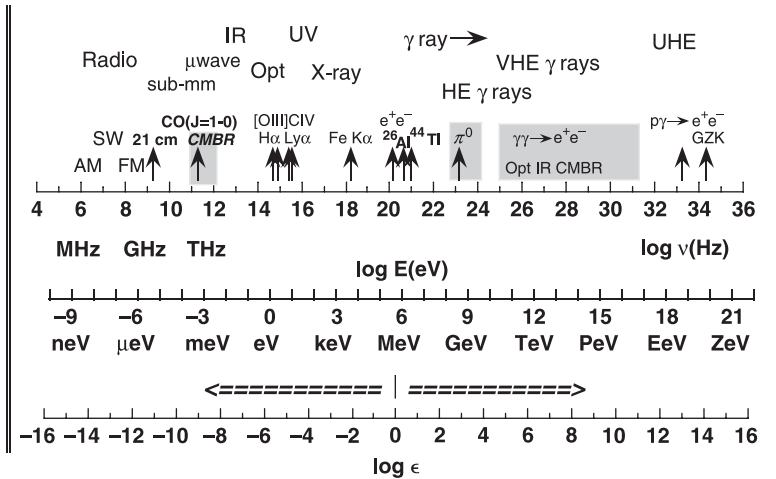


Figure 1.1 Photon and relativistic particle energy spectrum. Shown are photon or particle energies in units of Hz, eV, and electron rest mass ($\epsilon = hv/m_e c^2$), and some important astronomical lines and features. The mean energy of a cosmic microwave background (CMB) photon at the present epoch, in units of electron rest mass, is $\approx 10^{-9}$.

temperature and proton Thomson depth [8]. Photons exceeding many tens of MeV, or hundreds of MeV from pionic emissions of thermalized protons, must therefore originate from nonthermal processes. The existence of cosmic rays and GeV–TeV γ -ray sources attests to the importance of non-thermal processes throughout the universe.

The Electromagnetic Spectrum

During the past ~ 75 years,⁴ the cosmic *electromagnetic spectrum* outside the visual domain has been explored using telescopes with different limiting sensitivities and imaging capabilities over the range of frequencies ν (Hz) extending from ≈ 30 kHz to $\nu = 10^{27}$ Hz (i.e., photon energies $E = 10$ TeV); see figure 1.1. Absorption by interplanetary plasma limits observations from space-based radio detectors below ≈ 30 kHz, and the Earth’s ionosphere hampers observations of cosmic radio emission below ≈ 10 – 30 MHz frequencies. The sky is transparent at higher radio frequencies and in the optical waveband. Space research overcomes the limitations of the obscuring atmosphere in many wavelength ranges.

Ultraviolet and X-ray fluxes from compact sources are often attenuated by photoelectric absorption from intervening neutral or ionized matter,

⁴Karl Jansky discovered radio emission from the Galaxy in 1932.

including absorption by Milky Way gas. At TeV energies, the universe becomes opaque to pair production attenuation of very high-energy photons (γ) on cosmic infrared photons (γ'). This process, represented by the reaction $\gamma\gamma' \rightarrow e^+e^-$, prevents us from seeing extragalactic sources of multi-TeV radiation at distances ~ 1 Gpc (redshifts $z \sim 0.2$). The highest-energy cosmic photon yet detected was at ≈ 90 TeV from a Milagro source [9]. At 100 TeV energies and higher, telescopes yet lack sufficient sensitivity to detect cosmic sources or the plane of our Galaxy.

It is convenient to express the total energy E_γ of a photon in units of the electron rest-mass energy $m_e c^2$. The dimensionless energy of a photon with frequency ν is denoted by

$$\epsilon \equiv \frac{E_\gamma}{m_e c^2} = \frac{h\nu}{m_e c^2}. \quad (1.2)$$

The units of $m_e c^2$ give the energy units (table 1.1) of E_γ . The term ϵ in eq. (1.2) can also denote the dimensionless energy of highly relativistic ($\gamma \gg 1$) particles, such as cosmic rays or neutrinos. At nonrelativistic ($\gamma - 1 \ll 1$) and transrelativistic ($\gamma - 1 \approx 1$) particle energies, the total energy, kinetic energy, and momentum must be more carefully related than in the ultrarelativistic regime, where $p = \sqrt{\gamma^2 - 1} \rightarrow \gamma$ when $\gamma \gg 1$. Figure 1.1 illustrates the energy scale of astronomical photon observations in Hz, eV, and dimensionless units.

The Astroparticle Spectrum

Cosmic rays consist of nonthermal protons, ions, electrons, positrons, photons, and antiprotons. Intensities of various cosmic-ray ionic components, multiplied by $E^{2.75}$, are shown in the left panel in figure 1.2. The dashed line gives the approximation $I_p(E) = 2.2E^{-2.75}$ protons/(cm² s GeV sr) multiplied by $E^{2.75}$ (therefore a straight line in this plot) to the demodulated flux of cosmic-ray protons, valid from $E \sim 1$ GeV to $\approx 10^{14}$ eV. Note that α -particles and heavier nuclei make an increasing contribution to the cosmic-ray flux near the knee of the cosmic ray spectrum at ≈ 3 PeV.

At the lowest energies of the nonthermal particle spectrum, Solar energetic particles accompanying Solar flares and coronal mass ejections have been measured with energies ranging from keV/nucleon to GeV/nucleon. Cosmic rays from outside our Solar system range in energy from directly detected \sim GeV/nucleon cosmic-ray ions, at lower energies, to air shower and fluorescence events with energies exceeding 10^{20} eV at high energies. For energies \sim few GeV/nucleon, the cosmic-ray flux varies with the phase of the 11-year Solar sunspot cycle. This Solar modulation of the low-energy

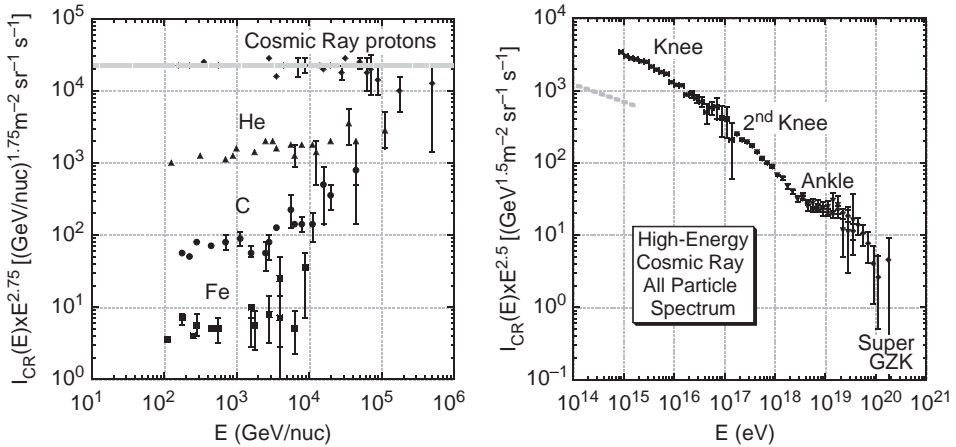


Figure 1.2 *Left panel:* Cosmic-ray number intensity multiplied by $E^{2.75}$ for cosmic-ray ions with energy $E \lesssim 10^{14}$ eV/nucleon. *Right panel:* Cosmic-ray number intensity multiplied by $E^{2.5}$ for all cosmic rays with total energy $E \gg 10^{14}$ eV. Features of the high-energy cosmic-ray all-particle spectrum are identified.

cosmic-ray flux results from adiabatic losses of the cosmic rays as they penetrate the heliosphere and diffuse through the outflowing Solar wind.

The heliosphere does not significantly perturb trajectories of cosmic rays with $E \lesssim 10$ GeV/nucleon, and these cosmic rays sample the interstellar cosmic-ray flux. In a magnetic field with intensity B , the Larmor radius of a particle with mass m , atomic mass A , and charge Z is

$$r_L \cong \frac{mc^2 \beta_{\text{par}} \gamma}{QB} \xrightarrow{\gamma \gg 1} \frac{E}{ZeB} \cong 1.1 \frac{E (\text{PeV})}{ZB (\mu\text{G})} \text{ pc} \cong \frac{A}{Z} \left(\frac{m}{m_p} \right) \frac{m_p c^2}{eB} \gamma$$

$$\cong \begin{cases} \frac{1706}{B (\text{G})} \gamma \text{ cm}, & \text{electrons,} \\ \frac{3.13 \times 10^6 A}{ZB (\text{G})} \gamma \text{ cm} \cong \frac{A/Z}{B (\mu\text{G})} \left(\frac{\gamma}{10^6} \right) \text{ pc} & \\ \cong \frac{E (10^{20} \text{ eV})}{ZB (10^{-10} \text{ G})} \text{ Gpc}, & \text{protons or ions.} \end{cases} \quad (1.3)$$

Particles with $r_L \gg R$ will escape from or penetrate into a region of size R with mean magnetic field B , and will do this on the light crossing timescale R/c . Cosmic-ray protons with energies $E \gtrsim 10^{17}$ eV, well above the knee energy at ≈ 3 PeV, have Larmor radii comparable to the ≈ 180 pc thickness of the Galaxy's disk. At such energies, cosmic-ray protons originating in the disk of the Galaxy will escape into the halo of the Galaxy and escape

to intergalactic space. If formed beyond the Galaxy, such energetic cosmic rays can pass through the Galactic halo and into the Galaxy's disk.

The intensity of all cosmic-ray particles, irrespective of type, multiplied by $E^{2.5}$, is shown for $E \gg 10^{14}$ eV cosmic rays in the right panel of figure 1.2. Features of the high-energy spectrum are labeled. At the highest particle energies, extending from ultrahigh energies (UHE; 10^{18} eV) to super-GZK energies ($> 10^{20}$ eV),⁵ the different signatures of the air showers formed by a photon and a particle are not clear cut, and depend on the particle physics model used to interpret air show data [12]. The Auger collaboration report [13] that the photon fraction of the UHECR (ultrahigh-energy cosmic ray) flux at $E \cong 10^{19}$ eV is $\sim 2\%$. The Auger result [14] on clustering of arrival directions of $\sim 6 \times 10^{19}$ eV UHECRs rules out a Galactic origin, and the large gyroradii and near isotropy of cosmic rays with $E \sim 4 \times 10^{19}$ eV also suggest an extragalactic origin. The energy of the transition from a Galactic disk or halo component to an extragalactic component, assuming there is a definite transition energy, could be at the second knee or at the ankle, and is an open question.

High-energy neutrinos make up another important component of the astroparticle spectrum.⁶ The high-energy nonthermal neutrino window is being opened in this decade with observations from \sim TeV to 10^{20} eV. Various estimates [16] suggest that detection of 100 TeV–100 PeV neutrinos from cosmic sources is probable with neutrino telescopes at the km scale, such as the IceCube experiment at the South Pole or a northern hemisphere neutrino telescope in the Mediterranean Sea. High-energy neutrino observations will be crucial to identify cosmic-ray accelerators and buried nonthermal sources.

The Gravitational-Wave Spectrum

The gravitational-wave spectrum offers a new window into the universe of high-energy activity. Distortions in spacetime induced by extreme events involving, for example, the coalescence of Solar mass neutron stars and black holes, induce minute strains on underground bars like those in the *Laser Interferometer Gravitational Wave Observatory* (LIGO). Relative displacements of the three-detector space-based array that forms the proposed *Laser Interferometer Space Antenna* (LISA) will be used to monitor

⁵GZK stands for Greisen, Zatsepin, and Kuzmin, an American and two Russian scientists who first pointed out that $\gtrsim 10^{20}$ eV cosmic rays would rapidly lose energy due to photohadronic interactions with the photons of the cosmic microwave background radiation (CMBR) [10,11]. See chapter 9.

⁶MeV neutrinos formed by nuclear burning in stars [15] or in dense collapsed cores of exploding stars are not treated here.

coalescence of massive black holes. LIGO is now taking data at its design sensitivity, and LISA may be developed as a NASA mission in the 2010–2020 time frame or later. Template gravitational waveform studies of merging compact objects and coalescing black holes will be a crucial tool to compare with data from these detectors. This subject, though of potentially great importance to black-hole physics, will not be treated here (see, e.g., Ref. [17]).

1.2 ENERGY FLUXES

Flux density F_ν is usually reported by radio astronomers in units of Jansky ($1 \text{ Jy} = 10^{-23} \text{ ergs cm}^{-2} \text{ s}^{-1} \text{ Hz}^{-1}$), so that the quantity νF_ν is an energy flux Φ (units of $\text{ergs cm}^{-2} \text{ s}^{-1}$, or Jy Hz , noting that $10^{10} \text{ Jy Hz} = 10^{-13} \text{ ergs cm}^{-2} \text{ s}^{-1}$). The luminosity distance d_L for a steady, isotropically emitting source is defined so that the energy flux Φ is related to the source luminosity L_* (ergs s^{-1}) according to the Euclidean expression

$$\Phi = \frac{L_*}{4\pi d_L^2} \quad (1.4)$$

(see chapter 4).

If $\phi(\epsilon)$ is the measured spectral photon flux (units of photons $\text{cm}^{-2} \text{ s}^{-1} \epsilon^{-1}$), then $\nu F_\nu = m_e c^2 \epsilon^2 \phi(\epsilon)$. Henceforth we use the notation

$$f_\epsilon = \nu F_\nu \quad (1.5)$$

for the νF_ν flux. From the definitions of Φ and f_ϵ ,

$$\Phi = \int_0^\infty d\epsilon \frac{f_\epsilon}{\epsilon}. \quad (1.6)$$

From eq. (1.4), the luminosity radiated by a source between measured photon energies ϵ_1 and ϵ_2 , or between source frame photon energies $\epsilon_1(1+z)$ and $\epsilon_2(1+z)$, is given by

$$L_*[\epsilon_1(1+z), \epsilon_2(1+z)] = 4\pi d_L^2 m_e c^2 \int_{\epsilon_1}^{\epsilon_2} d\epsilon \epsilon \phi(\epsilon) = 4\pi d_L^2 \int_{\ln \epsilon_1}^{\ln \epsilon_2} d(\ln \epsilon) f_\epsilon. \quad (1.7)$$

Equation (1.7) shows that if the νF_ν spectrum is flat with value f_ϵ^0 , corresponding to a photon flux $\phi(\epsilon) \propto \epsilon^{-2}$, then the apparent power of the source over one decade of energy is $\approx (\ln 10) L_0 \approx 2.30 L_0$, where $L_0 = 4\pi d_L^2 f_\epsilon^0$.

Long-duration GRBs are thought to be powered by the core collapse of massive stars to black holes [18]. A large fraction is detected at cosmological distances, that is, at mean redshifts $\langle z \rangle \approx 1$; thus their mean apparent isotropic γ -ray energy releases are

$$\mathcal{E}_* = \frac{4\pi d_L^2 \Phi \langle \Delta t \rangle}{(1+z)} \approx 10^{51} \frac{d_{28}^2}{(1+z)/2} \frac{\Phi}{10^{-7} \text{ ergs cm}^{-2} \text{ s}^{-1}} \frac{\langle \Delta t \rangle}{20 \text{ s}} \text{ ergs}, \quad (1.8)$$

where $d_L = 10^{28} d_{28}$ cm, $d_{28} \approx 2$ for a GRB at $z = 1$, and the mean duration $\langle \Delta t \rangle \approx 20$ s. The factor $1+z$ relates the observer time to the source frame time.

Blazars are thought to be supermassive black-hole sources with jets, oriented such that we are viewing nearly along the jet axis. The jet emission is strongly amplified by Lorentz-boosting of relativistic outflows, so that we can see such sources to high redshift. One such blazar is the bright flat-spectrum quasar PKS 0528 + 134 at $z = 2.06$ ($d_{28} \cong 5$). During bright γ -ray states discovered with the Energetic Gamma Ray Experiment Telescope (EGRET) on the *Compton Gamma Ray Observatory*, its apparent isotropic γ -power exceeded $\sim 10^{49}$ ergs s^{-1} [19]. The bright blazar 3C 279 at $z = 0.538$ ($d_{28} \cong 1$) also flares with apparent γ -ray luminosity 10^{49} ergs s^{-1} [20]. Such flares, lasting for hours to days, involve apparent isotropic energy releases $\sim 10^{53}$ ergs.

The relative magnitude of two sources with magnitudes m_1 and m_2 is defined as

$$m_1 - m_2 = -\frac{5}{2} \log \frac{\Phi_1}{\Phi_2}, \quad (1.9)$$

where $\Phi_{(\nu)} = L_{*(\nu)}/4\pi d_L^2$ is the (spectral) energy flux, and $\Phi_{(\nu)}$ and $L_{*(\nu)}$ are in cgs units of ergs $\text{cm}^{-2} \text{ s}^{-1}$ (Hz^{-1}) and ergs s^{-1} (Hz^{-1}), respectively. Five magnitudes correspond to a factor 10^2 in relative energy fluxes.

Table 1.2 gives a reference optical magnitude scale [21] and the spectral energy flux $\Phi_\nu(0)$ of a zeroth magnitude star, converted to νF_ν energy fluxes $f_\epsilon(0)$ at that photon frequency. The energy flux of a zeroth magnitude star in the V band is about 10^{11} times fainter than the Solar constant ($\cong 1 \text{ kW m}^{-2}$; see Appendix E) and $\approx 10^{10}$ times brighter than a 25th magnitude galaxy (in V), which has an energy flux $\Phi \approx 10^{-15}$ ergs $\text{cm}^{-2} \text{ s}^{-1}$. The largest optical telescopes detect galaxies with $m = 30$, and therefore reach sensitivities $\Phi \approx 10^{-17}$ ergs $\text{cm}^{-2} \text{ s}^{-1}$. The *Hubble Space Telescope* only reaches R magnitude $m_R \cong 25$ because of its smaller mirror compared to ground-based telescopes, but its imaging is magnificent at $\sim 0.1''$.

Table 1.2 Reference Optical Magnitude Scale^a

Filter	λ_0 (μ)	ν (10^{14} Hz)	E_γ (eV)	ϵ (10^{-6})	$\Phi_\nu(0)$	$f_\epsilon(0)$
					($\text{kJy} = 10^{-20}$ $\text{ergs/cm}^2 \text{ s Hz}$)	($\text{ergs/cm}^2 \text{ s}$)
U	0.365	8.22	3.40	6.78	1.9	1.56×10^{-5}
B	0.44	6.82	2.82	5.52	4.27	2.91×10^{-5}
V	0.56	5.40	2.24	4.38	3.54	1.91×10^{-5}
R	0.7	4.28	1.77	3.47	2.84	1.21×10^{-5}
J	1.25	2.40	0.99	1.94	1.60	3.83×10^{-6}
L	3.45	0.87	0.36	0.70	0.29	2.52×10^{-7}
M	4.8	0.62	0.257	0.50	0.163	1.02×10^{-7}

^aFlux density $\Phi_\nu(0)$ and νF_ν flux $f_\epsilon(0)$ for a zeroth magnitude star; the precise scale depends on the photometry system, filter, and bandwidth. For instance, Johnson V magnitude has central wavelength $\lambda_0 = 0.545 \mu\text{m} = 5450 \text{ \AA}$ and a bandwidth of 880 \AA .

1.3 TIMING STUDIES AND BLACK-HOLE MASS ESTIMATES

The Schwarzschild radius of a black hole of mass M is

$$R_S = \frac{2GM}{c^2} \cong 3.0 \times 10^5 \frac{M}{M_\odot} \text{ cm}, \quad (1.10)$$

and $R_S \approx 2 \text{ AU}$ for a $10^8 M_\odot$ black hole. To resolve the nuclear region of a cosmologically distant black hole within $\approx 10^2 R_S$ requires an imaging capability of $\approx 10^{-14}$ rad, which is beyond present technical ability. The mass of the black hole at the Galactic Center, inferred from analysis of stellar orbits, is $M_{\text{GC}} \approx 4 \times 10^6 M_\odot$ [22,23]. The Very Large Baseline Array (VLBA) has an imaging capability of $\approx 10^{-9}$ rad, sufficient to establish the source size of 42 GHz radio emission to $24(\pm 2) R_S$ [24]. The Galaxy's central black hole is the best candidate to directly image the inner regions of a black hole.

Lack of sufficient angular resolution to resolve the different radiating regions near a black hole can in principle be remedied through analysis of time histories of count or photon data. Variations in the source flux by a large factor (> 2) over a time scale Δt must, from causality arguments for stationary sources, originate from an emission region of size $R \leq c\Delta t/(1+z)$. If the radiation were emitted from larger size scales, incoherent superposition of emissions from regions that are not in causal contact would smooth large-amplitude fluctuations. For high-quality data from bright flares, large-amplitude variations in source flux on timescale Δt would, from

this argument, imply a black-hole mass

$$\frac{M}{10^9 M_\odot} = \frac{\Delta t}{(1+z)10^4 \text{ s}}. \quad (1.11)$$

The measured size scale $R = c\Delta t/(1+z)$ reflects the physical dimensions of the energy generation region, but not necessarily the distance of the emission site from the source. For emission regions in relativistic motion with bulk Lorentz factor Γ , the actual location of the emission region can be as far as $\approx \Gamma^2 c\Delta t/(1+z)$ from the explosion center (see chapter 5). *High Energy Stereoscopic System* (HESS) detection of rapid $\sim 0.2\text{--}2$ TeV flares from PKS 2155-304 on timescales ~ 300 s, much shorter than the light crossing time across a black hole of $\approx 10^9 M_\odot$ thought to be found in this system [25], is therefore surprising [26].

There are a wide range of methods to determine the masses of Galactic and extragalactic black holes. The most reliable methods employ direct measurements of stellar or gaseous velocities in the vicinity of the black hole, or reverberation mapping of emission lines of surrounding gas in response to changes in the UV flux of the central nucleus [3]. The mass of the black hole and the mass of the bulge of the host galaxy are found to correlate in the ratio of $\approx 1 : 500$ with small, factor-of-2 scatter [27].⁷ For supermassive black holes at large redshifts where the host galaxy cannot be resolved, timing studies could offer the best hope to measure black-hole mass. Black-hole masses have been determined from analysis of X-ray data, but how precisely to determine the black-hole mass from variability data at γ -ray energies remains unclear.

1.4 FLUX DISTRIBUTION

A valuable tool for studying properties of steady or flaring sources is the statistical distribution of fluxes or fluences, called the flux (or $\log N\text{--}\log S$) distribution. The observable quantity could be peak flux within a given photon waveband, flux averaged over a long observing timescale, or fluence of a blazar flare or GRB. Expressing the sensitivity of a high-energy radiation detector in terms of a threshold flux Φ_{thr} imposes the condition that $\Phi \geq \Phi_{\text{thr}}$. For unbeamed sources with luminosity L_* and distance d ($\cong d_L$ at low redshifts), $\Phi = L_*/4\pi d^2$, and the maximum source distance for a give source flux Φ is

$$d(\Phi) = \sqrt{\frac{L_*}{4\pi\Phi}}.$$

⁷A later study [28] shows a ratio of $\approx 1 : 800$ for black holes in 72 AGNs, with more than 50% of the sample within a factor of 3 of the best-fit relation.

Hence the flux distribution for sources that are uniformly distributed with density n_0 in flat space is

$$N(>\Phi) = N(<d) = 4\pi n_0 \int_0^{d(\Phi)} dx x^2 \propto \Phi^{-3/2}, \quad (1.12)$$

as is well known.

The $\langle V/V_{\max} \rangle$ statistic [29]

$$\langle V/V_{\max} \rangle = \frac{1}{N} \sum_{i=1}^N \frac{\Phi_i}{\Phi_{\text{thr}}}^{-3/2} \quad (1.13)$$

expresses the deviation from 0.5 expected for a uniform Euclidean distribution of sources. Here V stands for volume, and V_{\max} is the maximum volume from which a source with flux Φ could be detected. Values of $\langle V/V_{\max} \rangle > 0.5$ represent positive evolution of sources, that is, either more sources and/or brighter sources at large distances or earlier times. Values of $\langle V/V_{\max} \rangle < 0.5$ represent negative source evolution, i.e., fewer or dimmer sources in the past. Detailed treatments of the statistical properties of black hole sources must consider cosmological effects and evolution of source properties.

Analysis of the statistics of the sources of UHECRs, needed for charged particle astronomy [14], is complicated by the unknown strength and geometry of Galactic and intergalactic magnetic fields.

1.5 THE NIGHTTIME SKY

Intergalactic space is permeated by a background glow made up of stellar and black-hole radiations, and the remnant CMBR left over from the big bang (figure 1.3). The mean intensity of light in intergalactic space is referred to here as the extragalactic background light, or EBL. In terms of energy density, the CMBR represents the dominant radiation field of the EBL in intergalactic space (see figure 1.3). The present temperature of the CMBR is 2.728 ± 0.004 K [31]. Other than the $\sim 0.1\%$ dipole anisotropy due to the Galaxy's proper motion, the CMBR shows deviations at 10^{-5} from a perfect blackbody due to acoustical imprints from the big bang.

The intensity of the diffuse background IR radiation field is difficult to measure directly because of foreground radiations, such as Galactic electron synchrotron radiation and zodiacal light scattered by dust in our Solar system. The optical component of the diffuse EBL traces, primarily, stellar radiation from spiral and elliptical galaxies. The IR component is primarily radiation from stars and black holes that has been reprocessed through large column densities of cold dust. The energy density of the dust and stellar components of the EBL is $\approx 10\%$ of the CMBR energy density at the present epoch.

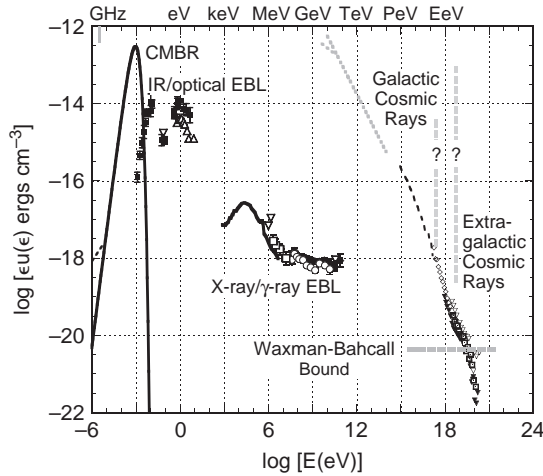


Figure 1.3 Spectral energy densities in intergalactic space of various radiations, including the CMB, the infrared (IR) and optical, X-ray, γ -ray, the extragalactic cosmic ray, and the predicted maximum energy density of cosmogenic neutrinos from photopion interactions of UHECRs with photons of the extragalactic background light (EBL) [30]. Also shown is the energy density of cosmic rays measured near Earth; the transition energy between the galactic and extragalactic components is uncertain.

The X-ray background is resolved from analysis [32] of observed populations into, primarily, Seyfert galaxies, which are star-forming (usually disk) galaxies with strong blue/UV excesses from central nuclei. Also making up the X-ray background is a significant contribution from “buried” black holes, namely accreting black holes with masses $\sim 10^5$ – $10^8 M_\odot$ that are surrounded by material with column densities exceeding $\sim 10^{24}$ H atoms cm^{-2} .

The identified extragalactic γ -ray sources in the EGRET (~ 100 MeV–10 GeV) range are blazars and GRBs. The superposition of faint blazar sources probably makes a significant contribution to the diffuse extragalactic γ -ray background [33,34] shown in figure 1.3. There are additional uncertain contributions from γ rays formed by cosmic rays accelerated in structure formation shocks, or in star-forming galaxies.